Gold Nanoparticles

DOI: 10.1002/ange.201402937

Dynamic and Quantitative Control of the DNA-Mediated Growth of Gold Plasmonic Nanostructures**

Jianlei Shen, Lifeng Xu, Chunpeng Wang, Hao Pei, Renzhong Tai, Shiping Song, Qing Huang, Chunhai Fan, and Gang Chen**

Abstract: *Reproducible and controllable growth of nanostructures with well-defined physical and chemical properties is a longstanding problem in nanoscience. A key step to address this issue is to understand their underlying growth mechanism, which is often entangled in the complexity of growth environments and obscured by rapid reaction speeds. Herein, we demonstrate that the evolution of size, surface morphology, and the optical properties of gold plasmonic nanostructures could be quantitatively intercepted by dynamic and stoichiometric control of the DNA-mediated growth. By combining synchrotron-based small-angle X-ray scattering (SAXS) with transmission electron microscopy (TEM), we reliably obtained quantitative structural parameters for these fine nanostructures that correlate well with their optical properties as identified by UV/Vis absorption and dark-field scattering spectroscopy. Through this comprehensive study, we report a growth mechanism for gold plasmonic nanostructures, and the first semi-quantitative revelation of the remarkable interplay between their morphology and unique plasmonic properties.*

Gold nanoparticles (AuNPs) have received considerable interest during the last several decades because of their fascinating optical, electronic, and catalytic properties. The properties of AuNPs can be easily tuned by tailoring their size and shape.[1] A variety of AuNPs with different sizes and shapes have been synthesized, including spheres,[2] cubes,[3] rods,[4] and prisms.[5] The optical properties of AuNPs with fixed shapes often have limited tunability as a result of the difficulty to control their size distribution and colloid stability. To address this issue, many unique gold nanostructures have been synthesized, for example, gold-coated silicon spheres with different shell thicknesses,[6] and spherical nanoparticles with various surface structures.[7] The nanoparticles with surface structure are termed multibranched nanoparticles and are usually called nanoflowers,[8] nanostars,[9] or urchin-like gold nanoparticles.[10] By controlling the petal number and shape of the nanoflowers, for instance, the optical properties of these nanostructures can be finely tuned with only a slight change to their sizes. Compared with spheres of similar size, gold nanostructures have highly tunable optical absorption bands that can extend to the near-red region.[11]

Highly branched gold nanostructures have shown attractive plasmonic properties because of the strong enhancement of the electromagnetic field surrounding their petals.[12] For instance, surface-enhanced Raman scattering (SERS) properties of gold nanostructures have been extensively explored because of their potential application in single-molecule detection.[13] In addition, gold nanostructures are used as drug transporters for gene therapy because of their large surface-to-volume ratio[14] and are also studied as catalysts.[15] However, because of their complex morphology, the synthesis of gold nanostructures is confronted with low reproducibility, which significantly restricts many of their potentially widespread applications. The quantitative elucidation of the underlying growth mechanism is key to addressing this problem. While there have been many studies in this context, the exact growth dynamics remain unknown. For example, aggregation-based nanocrystal growth is a potential mechanism which is still under debate.[16] This is mainly because of the limitation of the popularly employed transmission electron microscopy (TEM) technique, which requires pretreatment of samples and is prone to artifacts. Moreover, it is often difficult to obtain quantitative 3D structural parameters of fine nanostructures with TEM. To gain a more precise understanding of the nanostructure growth, we reasoned that synchrotron-based small angle X-ray scattering (SAXS) could be applied in addition to TEM. Samples for SAXS measurements can been investigated in situ, positioned in capillaries, or in levitated droplets without further preparation.

Recently, the genetic material, DNA, has been exploited to control the assembly[17] and growth of gold plasmonic nanostructures.[18] Herein, we developed a novel approach to dynamically and quantitatively control the DNA-mediated growth of a well-defined nanostructure with a uniform and hollow gap between its core and shell that can yield highly stable and reproducible SERS signals. By keeping the reducing agent in excess while controlling the concentration of gold ions added to the reaction solution, it was possible to halt the reaction at five successive stages and obtain five

[*] Dr. J. Shen, L. Xu, Dr. C. Wang, Dr. H. Pei, Prof.Dr. R. Tai, Prof.Dr. S. Song, Prof.Dr. Q. Huang, Prof.Dr. C. Fan, Prof.Dr. G. Chen
Shanghai Synchrotron Radiation Facility
Division of Physical Biology
CAS Key Laboratory of Interfacial Physics and Technology
Shanghai Institute of Applied Physics, Chinese Academy of Sciences
Shanghai 201204 (China)
E-mail: fchh@sinap.ac.cn
chengang@sinap.ac.cn

[**] This work was financially supported by the Ministry of Science and Technology of China (2013CB932803, 2012CB825805, and 2013CB933802) and the National Natural Science Foundation of China (11275251, 11179004, 11375256, 91313302, 21390414). G.C. acknowledges the support from the Hundred Talents project of the Chinese Academy of Sciences. We thank all the team members at BL16B1 of SSRF.

Supporting information for this article is available on the WWW under http://dx.doi.org/10.1002/anie.201402937.

different kinds of nanostructures varying in size and morphology. Given that the only changing parameter in each reaction was the quantity of the gold precursors added, the products can be considered as five intermediates in the formation of a fully grown nanostructure. Quantitative structural and optical measurements were carried out with SAXS, TEM, UV/Vis absorption spectroscopy, and dark-field microscopy. Through these comprehensive studies, a tenable growth mechanism was determined. The effect of the size and surface morphology of nanostructures on their overall (absorbance) and local (SERS) optical performance was systematically studied. Both experimental and theoretical results provided semiquantitative evidence that surface morphology played the key role in regulating the plasmonic properties of gold nanostructures.

X-ray measurements were carried out at the SAXS beamline (BL16B1) of the Shanghai Synchrotron Radiation Facility, with the incident X-ray photon energy at 10 keV and a MAR165 area detector. Experimental data and scattering background data were taken with and without gold nanostructures in solution. The procedure for sample preparation is shown in Figure 1 a. From stages one to five, hydroxylamine hydrochloride (10 μL of a 10 mM solution) was added to each of five solutions with DNA-coated AuNP seeds. Subsequently, 2 μL, 4 μL, 6 μL, 8 μL, and 10 μL, respectively, of chloroauric acid solutions (2% w/v) were added separately into the solutions (more details in the Experimental Section in the Supporting Information). As shown in Figure 1 b (SAXS image labeled "Au seeds"), there is no apparent scattering pattern for the DNA-coated AuNP solution within the detection region of our setup; with the addition of chloroauric acid solution, two scattering rings, a visible inner ring and a dim outer ring, emerge in the SAXS images. Both rings shrink in size and the outer ring is becomes clearer as the reaction progresses with increasing amounts of added chloroauric acid, indicating that the nanostructures have grown larger and smoother. By carefully subtracting scattering background data from the raw data and integrating along the equal wavevector transferring rings, one-dimensional scattering data is obtained (Figure 1 c).

The cross-section of our gold plasmonic nanostructure model is displayed in Figure 1 d. Applying the core–shell model calculation,[19] we find the X-ray scattering amplitude from the nanostructure can be written as [Eq. (1)]

$$F(q) = \frac{4}{3}\pi r_e \rho_0 r_c^3 \Phi(qr_c) + \frac{4}{3}\pi r_e \rho_g \left[r_s^3 \Phi(qr_s) - r_c^3 \Phi(qr_c)\right] + \frac{4}{3}\pi r_e \rho_0 \left[r_0^3 \Phi(qr_0) - r_s^3 \Phi(qr_s)\right] + \pi r_e \rho_0 N a^2 \int_{r_0}^{r_0+b} \left[1 - \frac{(r-r_0)^2}{b^2}\right]\left[\frac{\sin(qr)}{qr}\right] dr \quad (1)$$

where r_c, r_s, and r_0 are the radii of the inner core and the inner and outer radii of the shell; N, a, and b are the number of ellipsoidal petals on the surface and the length of their semiaxes; r_e is the Thomson scattering length; ρ_0 and ρ_g are the effective electron densities of the nanostructure and its gap, and in this case they are the difference between the electron densities of gold and DNA with water. The $\Phi(x)$ function in Equation (1) is given by [Eq. (2)]

$$\Phi(x) = 3\frac{\sin x - x\cos x}{x^3} \quad (2)$$

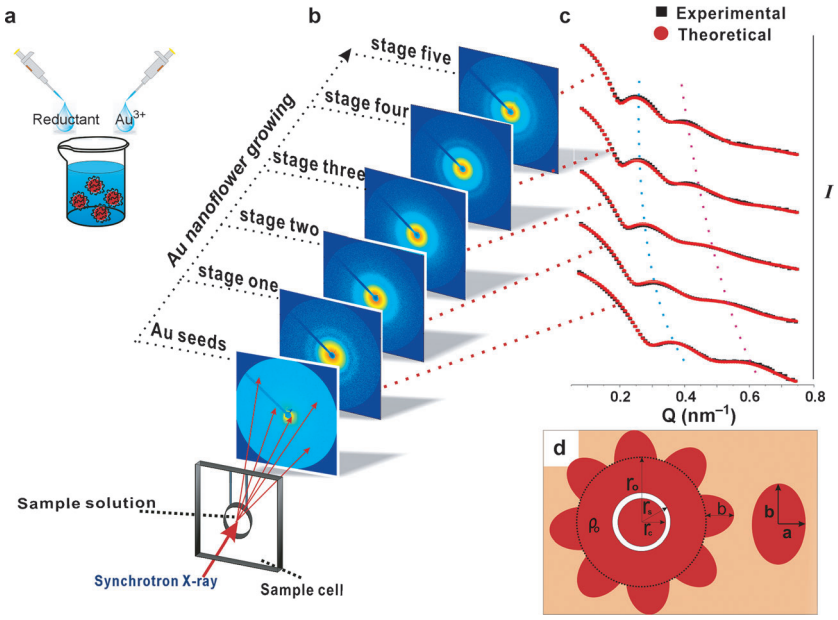

Figure 1. SAXS measurements and the structure model. a) Procedure for sample preparation. b) SAXS images of Au nanostructure samples at five successive growth stages prepared under stoichiometric control. c) One-dimensional SAXS data obtained by integrating the scattering patterns along equal wavevector transferring rings and their corresponding model fittings. d) Schematic view of the cross-section of the Au plasmonic nanostructure.

The detectable X-ray scattering intensity, $I(q)$, is the total summation of the modulus square of $F(q)$ multiplied by their corresponding statistical probability resulting from the size distribution of nanostructures [Eq. (3)]

$$I(q) = \int |F(q)|^2 G(r) dr \quad (3)$$

where $G(r)$ is the Gaussian distribution, $G(r) = \left(1/\sigma\sqrt{2\pi}\right)e^{-\frac{(r-\mu)^2}{2\sigma^2}}$, of the outer shell radius r_0 with two variables, the mean value μ and the standard deviation σ. A global optimization algorithm called covariance matrix adaptation evolution strategy (CMAES)[20] is used to optimize the model parameters. As shown in Figure 1 c, the experimental data and the corresponding model fits are in good agreement with the structural parameters listed in Table 1.

From stages one to three, the nanostructures continuously grow in size with the mean value μ of the outer shells increasing from 11.8 to 16.5 nm, while their size distribution becomes broader as indicated by the increasing of the standard

Table 1: The gold nanostructure model parameters at five successive growth stages [nm].

Parameter	Stage one	Stage two	Stage three	Stage four	Stage five
a	6.8	8.8	9.9	12.0	–
b	4.5	4.5	5.0	1.7	–
N	18.4	19.3	18.9	19.0	–
r_c	8.2	8.6	8.9	8.4	8.4
μ	11.8	14.3	16.5	20.2	22.6
σ	2.2	2.8	3.2	3.0	2.6

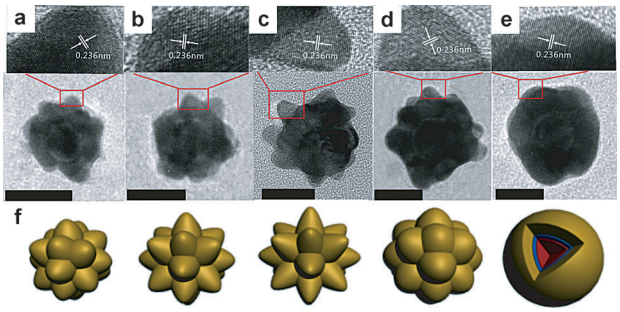

Figure 2. TEM measurements of Au nanostructures at five successive growth stages. a–e) High-resolution TEM images of the petals at growth stage one to five. f) Three-dimensional schematic representation of the size and morphological evolution of gold nanostructures during their growth. The final model shows the cross-section of the inner core, the gap, and the outer shell.

deviation σ (Table 1). Meanwhile, the base of the petals, a, expands from 6.8 to 9.9 nm while their length, b, does not change much and stays between 4.5 and 5.0 nm. Stage four is the turning point for both the nanostructure surface morphology and size distribution. At this stage, the petals become dramatically shorter (from 5.0 to 1.7 nm), hence the surface of the nanostructures become effectively smoother. The statistically averaged petal number, N, remains around 19 during the first four stages of growth. These results suggest that gold atoms are first deposited on the AuNP seeds where there is a low concentration of DNA and petals are produced from the surface. With increasing amounts of gold ion precursor, the petals grow larger and become blunter while their numbers do not change. Finally, the neighboring petals merge into one to form a smooth shell. At stage five, there are no obvious petals on the surface, which has a smooth shell with an averaging radius, μ, of 22.6 nm. During the model fitting process, the gap between the core and shell is set at 1 nm, which is consistent with the previous report[21] and confirmed in our samples by TEM measurements. This well-defined gap is formed as a result of the DNA coverage on AuNP seeds that prevents Au ion deposition; therefore its size is only determined by the natural width of the DNA chain.[22]

The TEM images (Figure S1, Supporting Information) are gold nanostructures obtained at five stoichiometrically controlled growth stages with different quantities of gold-ion precursors added to the reaction solution. Figure S1 provides a clear view of the size and surface morphology transformation which occurs during nanostructure growth. The diameters of gold nanostructures shown in Figures S1a–e (Supporting Information) are 33.1 ± 4, 38.4 ± 5, 43.4 ± 5, 44.2 ± 5, and 46.5 ± 5 nm, respectively. From the model shown in Figure 1d, the nanostructure diameter is equal to $2(r_0 + b)$ and its statistical mean value is $2(\mu + b)$. From Table 1, the diameters at growth stages one to five are equal to 32.6, 37.6, 43.0, 43.8, and 45.2 nm, respectively. The values obtained from TEM measurements are in good agreement with those obtained from SAXS measurements. The statistical size distributions are shown in the top insets of Figure S1 with the curves from SAXS model fittings drawn on top of the histograms obtained from TEM images. In these images, every particle has a uniform and hollow gap (1 nm) surrounding the inner core. This gap is visible when the shell is thin but becomes difficult to find when the shell thickness increases. To obtain a clear view of the gap, the scanning transmission electron microscopy (STEM) image in Figure S1 f is taken for the same sample as that in Figure S1 e.

The high-resolution TEM images in Figures 2a–e indicate that the single petals protruding from the surface of the gold nanostructures are monocrystalline while the entire nanostructure is polycrystalline. The 0.236 nm spacing highlighted in these images between the fringes belongs to the interplanar distance of gold (111) crystal planes. This further supports our conjecture that the petals grow independently and later merge to form a smooth shell. Summarizing the results from the SAXS and TEM measurements, the size and morphological evolution of gold plasmonic nanostructures can be schematically illustrated (Figure 2f). Initially, small round petals grow from the surface of the DNA-covered AuNP seed to form a thin and rough shell. The shell continues to grow and eventually becomes smooth and uniform once the petals have gone through the growth and decay process. The petals broaden in the first three stages without much change to their length, but they become significantly shorter at stage four; meanwhile the petal number does not change noticeably in the first four stages.

The UV/Vis absorption spectra of five successively grown gold nanostructures are shown in Figure 3a. As the amount of gold ion precursors added to the reaction solution increases, the absorption peak shifts to longer wavelengths (red shift), but at stage four, where 8 μL of gold precursor is added, it starts to shift to shorter wavelengths (blue shift). It is established that the absorption peak of AuNPs undergoes a red shift with increasing particle size.[23] In our case, the fully grown nanostructures (stage five) have a UV/Vis absorption peak (blue line in Figure 3a) at higher energy than the absorption peak for the stage one nanostructures (yellow line). From SAXS and TEM measurements, we know the diameters of the nanostructures in the corresponding solutions are approximately 33 and 45 nm, respectively. Since the solution environment is the same, the cause of the blue shift is attributed to the modification of surface morphology. Previous studies have reported that surface textures favor the red shift of the nanoparticle absorption band.[16b] Therefore, in our system there are two competing factors, particle size and surface texture, which affect the optical properties of the nanostructures. On the one hand, increasing the nanostructure size will cause the absorption maximum to red shift; on

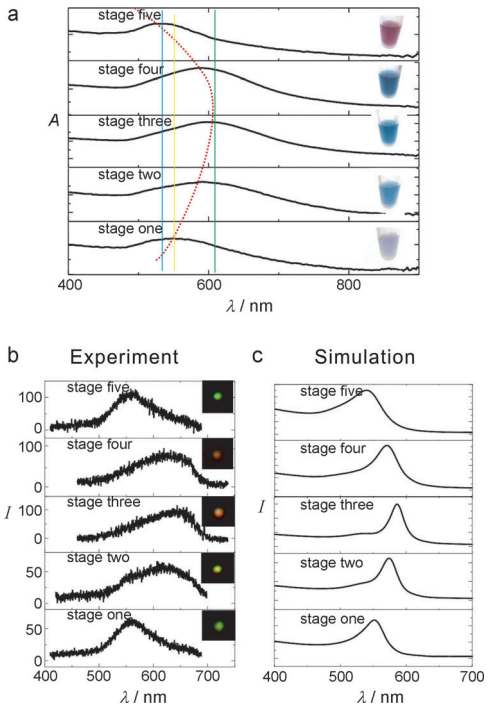

Figure 3. Optical measurements and FDTD simulations. a) The UV/Vis absorption spectra of Au nanostructure solutions taken at five successive growth stages. The yellow, green, and blue lines represent the peak positions of the UV/Vis absorption spectra of the Au nanostructures at stages one, three, and five, respectively. The red-dotted line is the trajectory of the maxima of the UV/Vis absorption spectra at different growth stages. b) The experimental and (c) theoretical dark-field scattering spectra of single Au nanostructures. The insets in (a) and (b) are the images of the solution samples and the dark-field microscopic view of single Au nanostructures, respectively. The spectra from bottom to top correspond to the growth stage one to five, respectively.

the other hand, smoothing their surface will lead to a blue shift. Based on these results, we find that the plasmon absorption bands of gold nanostructures are more sensitive to the length and sharpness of petals but less to the overall nanostructure size. It is also observed that the gold nanostructure solutions change their color at different stages as shown in the insets of Figure 3a. The solution color is complementary to the wavelength of the UV/Vis absorption band. The measurements presented in Figure 3b were carried out with dark-field microscopy. They show the same trend as that observed in the UV/Vis spectra, that is the peaks in the dark-field scattering spectra undergo a blue shift, following a series of red shifts, as the growth proceeds. To better understand the measured optical features in Figure 3a and b, theoretical simulations were carried out using the finite-difference time-domain (FDTD) method,[24] which has proven particularly useful for describing isolated nanoparticles of arbitrary shape in any defined surrounding environment. The parameters for the simulation were collected from the SAXS and TEM measurements. The overall profiles of the simulated spectra in Figure 3c are in good agreement with the experimental data in Figures 3a and b. Note, the small shoulders in the spectra of Figure 3 can be attributed to the weak dipole resonance of the inner core.[12,16b]

Previous studies have shown that plasmonic coupling between the inner core and the outer shell could cause a strong enhancement of the electromagnetic fields within the gap.[21] In spite of that, the influence of the size and morphology of the outer shell on the plasmonic behavior of nanostructures remains unexplored. It is established that the SERS signal is proportional to the fourth power of the electromagnetic field surrounding the nanostructure surface.[25] To measure SERS signals from gold nanostructures, the Raman reporter molecule, 4,4-dipyridyl, is loaded into the gap (details in the Experimental Section in the Supporting Information) and the solution is illuminated by incident light with a wavelength of $\lambda = 638$ nm. The Raman spectra for the nanostructures at five growth stages are recorded in Figure S2a. The integrated scattering peak intensities at 1612 cm^{-1} are plotted as a function of growth stage (Figure S2b). The near-field electromagnetic field distribution of the nanostructure is calculated using the FDTD method with the acquired structural parameters (Figure S2c). The fourth power of the electromagnetic field inside the nanostructure gap shows the same trend as that of the SERS signals (Figure S2b). As the shell thickness increases, the SERS signal from the Raman reporters inside the nanostructure gap increases steadily, but it decreases dramatically at stage five where the shell becomes smooth. These results clearly indicate that surface morphology, as compared to size, plays a dominating role in regulating the plasmonic effect of gold nanostructures.

The advance of nanoscience has seen the development of numerous functional nanostructures with fascinating physical and chemical properties. Nevertheless, current approaches for the preparation of nanostructures rely largely on empirical, time-consuming, and labor-intensive trial-and-error methods. To achieve dynamic and quantitative control of nanostructure preparation, we herein explored the DNA-mediated growth mechanism of gold plasmonic nanostructures, a process usually difficult to study because of their fast growth rate. By regulation of the stoichiometry in the reaction, we were able to break the nanostructure growth process into five consecutive stages, allowing a set of detailed structural and optical characterization techniques to be carried out. While TEM provides a powerful way to characterize nanostructures at the atomic level, it is a demanding task to retrieve quantitative 3D morphological information using the cryo-TEM and 3D reconstruction. In this study, we combined TEM with synchrotron-based SAXS to provide a simple and reliable way to attain quantitative structural information, for example the number of petals and particle-size distributions. By obtaining such structural parameters, a semiquantitative correlation between the morphology and plasmonic properties of these gold nanostructures could be established, which would otherwise be difficult with TEM characterization alone. In view of their broad practical applications and recent implementation in single-molecule detection, the ability to grow nanostructures with a specific morphology with specific optical and electronic properties has become increasingly important. DNA-mediated synthesis provides

a route to finely control the growth of these functional nanostructures. Our studies provide a novel approach to uncover the underlying growth mechanism and potentially to control the growth of gold plasmonic nanostructures and other functional nanostructures alike.

Received: March 3, 2014
Published online: June 20, 2014

Keywords: DNA · electron microscopy · gold nanoparticles · small-angle X-ray scattering · surface-enhanced Raman scattering

[1] Y. Xia, Y. Xiong, B. Lim, S. E. Skrabalak, *Angew. Chem.* **2009**, *121*, 62 – 108; *Angew. Chem. Int. Ed.* **2009**, *48*, 60 – 103.
[2] K. C. Grabar, R. G. Freeman, M. B. Hommer, M. J. Natan, *Anal. Chem.* **1995**, *67*, 735 – 743.
[3] A. R. Tao, S. Habas, P. D. Yang, *Small* **2008**, *4*, 310 – 325.
[4] T. K. Sau, C. J. Murphy, *Langmuir* **2004**, *20*, 6414 – 6420.
[5] J. E. Millstone, S. Park, K. L. Shuford, L. D. Qin, G. C. Schatz, C. A. Mirkin, *J. Am. Chem. Soc.* **2005**, *127*, 5312 – 5313.
[6] E. Prodan, C. Radloff, N. J. Halas, P. Nordlander, *Science* **2003**, *302*, 419 – 422.
[7] J. Rodríguez-Fernández, A. M. Funston, J. Pérez-Juste, R. A. Álvarez-Puebla, L. M. Liz-Marzán, P. Mulvaney, *Phys. Chem. Chem. Phys.* **2009**, *11*, 5909 – 5914.
[8] J. P. Xie, Q. B. Zhang, J. Y. Lee, D. I. C. Wang, *ACS Nano* **2008**, *2*, 2473 – 2480.
[9] a) C. L. Nehl, H. W. Liao, J. H. Hafner, *Nano Lett.* **2006**, *6*, 683 – 688; b) F. Hao, C. L. Nehl, J. H. Hafner, P. Nordlander, *Nano Lett.* **2007**, *7*, 729 – 732.
[10] O. M. Bakr, B. H. Wunsch, F. Stellacci, *Chem. Mater.* **2006**, *18*, 3297 – 3301.
[11] a) H. Wang, K. Fu, R. A. Drezek, N. J. Halas, *Appl. Phys. B* **2006**, *84*, 191 – 195; b) H. Wang, G. P. Goodrich, F. Tam, C. Oubre, P. Nordlander, N. J. Halas, *J. Phys. Chem. B* **2005**, *109*, 11083 – 11087.
[12] L. Rodríguez-Lorenzo, R. A. Álvarez-Puebla, I. Pastoriza-Santos, S. Mazzucco, O. Stéphan, M. Kociak, L. M. Liz-Marzán, F. J. García de Abajo, *J. Am. Chem. Soc.* **2009**, *131*, 4616 – 4618.
[13] H. Liu, L. Zhang, X. Lang, Y. Yamaguchi, H. Iwasaki, Y. Inouye, Q. Xue, M. Chen, *Sci. Rep.* **2011**, *1*, 112.
[14] D. H. M. Dam, J. H. Lee, P. N. Sisco, D. T. Co, M. Zhang, M. R. Wasielewski, T. W. Odom, *ACS Nano* **2012**, *6*, 3318 – 3326.
[15] H. G. Liao, Y. X. Jiang, Z. Y. Zhou, S. P. Chen, S. G. Sun, *Angew. Chem.* **2008**, *120*, 9240 – 9243; *Angew. Chem. Int. Ed.* **2008**, *47*, 9100 – 9103.
[16] a) A. Narayanaswamy, H. Xu, N. Pradhan, X. Peng, *Angew. Chem.* **2006**, *118*, 5487 – 5490; *Angew. Chem. Int. Ed.* **2006**, *45*, 5361 – 5364; b) L. Rodríguez-Lorenzo, J. M. Romo-Herrera, J. Pérez-Juste, R. A. Álvarez-Puebla, L. M. Liz-Marzán, *J. Mater. Chem.* **2011**, *21*, 11544 – 11549.
[17] a) E. Winfree, F. R. Liu, L. A. Wenzler, N. C. Seeman, *Nature* **1998**, *394*, 539 – 544; b) R. J. Macfarlane, B. Lee, M. R. Jones, N. Harris, G. C. Schatz, C. A. Mirkin, *Science* **2011**, *334*, 204 – 208; c) A. Kuzyk, R. Schreiber, Z. Fan, G. Pardatscher, E.-M. Roller, A. Hogele, F. C. Simmel, A. O. Govorov, T. Liedl, *Nature* **2012**, *483*, 311 – 314; d) S. J. Tan, M. J. Campolongo, D. Luo, W. Cheng, *Nat. Nanotechnol.* **2011**, *6*, 268 – 276.
[18] a) Z. Wang, J. Zhang, J. M. Ekman, P. J. A. Kenis, Y. Lu, *Nano Lett.* **2010**, *10*, 1886 – 1891; b) Z. Wang, L. Tang, L. H. Tan, J. Li, Y. Lu, *Angew. Chem.* **2012**, *124*, 9212 – 9216; *Angew. Chem. Int. Ed.* **2012**, *51*, 9078 – 9082.
[19] a) D. J. Yarusso, S. L. Cooper, *Macromolecules* **1983**, *16*, 1871 – 1880; b) G. Chen, M. A. Modestino, B. K. Poon, A. Schirotzek, S. Marchesini, R. A. Segalman, A. Hexemer, P. H. Zwart, *J. Synchrotron Radiat.* **2012**, *19*, 695 – 700.
[20] N. Hansen, A. Ostermeier, *Evol. Comput.* **2001**, *9*, 159 – 195.
[21] D.-K. Lim, K.-S. Jeon, J.-H. Hwang, H. Kim, S. Kwon, Y. D. Suh, J.-M. Nam, *Nat. Nanotechnol.* **2011**, *6*, 452 – 460.
[22] H. G. Hansma, I. Revenko, K. Kim, D. E. Laney, *Nucleic Acids Res.* **1996**, *24*, 713 – 720.
[23] P. K. Jain, K. S. Lee, I. H. El-Sayed, M. A. El-Sayed, *J. Phys. Chem. B* **2006**, *110*, 7238 – 7248.
[24] A. Taflove, Electromagnetic Compatibility, IEEE Transactions on. **1980**, EMC-22, 191 – 202.
[25] A. Campion, P. Kambhampati, *Chem. Soc. Rev.* **1998**, *27*, 241 – 250.

